Magnetic edge states of an impenetrable stripe

A. Matulis* and T. Pyragienė

Semiconductor Physics Institute, Goštauto 11, 2600 Vilnius, Lithuania
(Received 27 September 2002; published 27 January 2003)

The electron motion in a strong perpendicular magnetic field close to the impenetrable stripe is considered by making use of the singular integral equations technique. The energy spectrum is calculated and compared with the energy spectrum of the round antidot. It is shown that in the case of the long stripe, the eigenfunctions can be obtained as a superposition of magnetic edge modes, while the fractal energy levels obtained in a high-energy region can be explained from the quasiclassical point of view.

I. INTRODUCTION

Progress in a nanometer technology and the ability to tailor potentials has triggered a broad activity in low-dimensional semiconductor nanostructures. Among the 2D (two-dimensional) structures the quantum dots with the electrons confined in a small region have been a subject of the intense theoretical and experimental research during the past years.[1] The complete confinement and the discrete energy spectrum converted these objects into a useful instrument for the electron interaction and correlation studies.[2] In the strong perpendicular magnetic field the quantum antidot, the region with a repulsive potential, can bound the electrons as well. The magnetotransport experiments on the arrays of the quantum antidots[3] showed a close relation of the pronounced structure in the magnetoresistance and the periodic classical orbits, or the corresponding spectrum of the antidots. It was tested on the arrays of various shape antidots.[4] The importance of the antidot-bound electron states was confirmed in the studies of magnetotransport through clusters of the antidots[5] and the individual antidots.[6]

The spectrum of the quantum antidot in the magnetic field is also interesting from the dynamic chaos point of view (see Ref. 7 and references there). The quantum antidots together with quantum billiards are the most simple and convenient structures for revealing the links between the autocorrelations in quantum spectrum and the periodic orbits of the classical problem. The most convenient technique for solving the antidot eigenvalue problems with not separating variables is the singular integral equations. Usually the sharp antidot edges increase the singularity of these equations making them rather complicated and even not useful. In this paper using the simplest antidot, the finite impenetrable line, we demonstrate how the integral equation technique can be used in the case of the antidot with the sharp edges. We have failed to find that this simple but revealing antidot spectrum has been considered ever before. Comparing this spectrum with the round antidot one we demonstrate the main features of the problem with nonseparable variables. The limit cases of a long antidot and high electron energy show the peculiarities of the quantized magnetic edge modes and the quasiclassical quantization.

The paper is organized as follows. In Sec. II the problem is formulated. In Sec. III the simplest ultrashort stripe case is considered, and in Sec. IV the numerical results for the energy spectrum are presented. In order to explain the physical meaning of the spectrum peculiarities, two limit cases—the long stripe in Sec. V and large electron energy in Sec. VI—are considered. In Sec. VII the conclusions are given, and in the Appendix the details related to the discretization of the singular integral equation are collected.

II. MODEL

We consider the electron moving in x-y plane which is shown in Fig. 1. The antidot, an infinitely thin impenetrable line $|x| \leq a/2$, $y = 0$, is indicated by the gray stripe. We solve the Schrödinger equation

$$\{H - E\}\Psi(\mathbf{r}) = 0, \tag{1}$$

with the following dimensionless Hamiltonian:

$$H = -\frac{1}{2}\{\nabla + i\mathbf{A}(\mathbf{r})\}^2, \tag{2}$$

where the perpendicular magnetic field is described by the vector potential in the symmetric gauge $\mathbf{A}(\mathbf{r}) = \{-y, x\}/2$. We use the following notation for 2D vectors $\mathbf{r} = \{x, y\}$. The energy is measured in $\hbar\omega_c$ ($\omega_c = eB/mc$) units, and the coordinates—in the magnetic length $l_B = \sqrt{c\hbar/eB}$ units. The antidot—the impenetrable stripe—is taken into account by a hard wall boundary condition

$$\Phi(\mathbf{r})\big|_{|x| \leq a/2, y = \pm 0} = 0. \tag{3}$$

Besides, the wave function satisfies zero boundary conditions at the infinity $\Psi(\mathbf{r})\big|_{r \to \infty} = 0$.
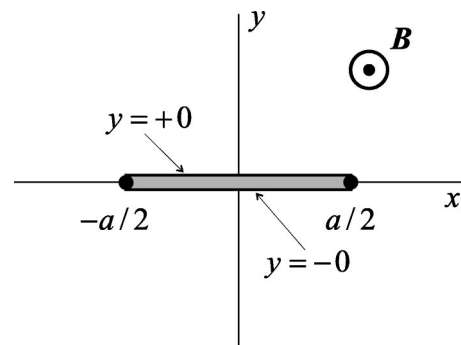

FIG. 1. Layout.

Making use of the Green's theorem the above two-dimensional problem can be transformed into a one-dimensional integral equation. Indeed, introducing the whole plane Green's function as a solution of the equation

$$\{H-E\}G(\mathbf{r}|\mathbf{r}')=-\delta(\mathbf{r}-\mathbf{r}'), \qquad (4)$$

and taking the boundary conditions $G(\infty|\mathbf{r}')=0$ into account, one can present the wave function as the integral (see the details in Ref. 7)

$$\Psi(\mathbf{r})=\frac{1}{2}\int_{-a/2}^{a/2}dx'\,G(\mathbf{r}|x',0)F(x') \qquad (5)$$

over the perimeter of the antidot. Here

$$F(x)=\Psi_y(x,+0)-\Psi_y(x,-0) \qquad (6)$$

is the difference of the wave-function derivatives on the opposite sides of the stripe. We shall refer to it as the perimeter function.

The wave function defined via Eq. (5) satisfies already Eq. (1) and the boundary condition at the infinity. Satisfying the boundary condition on stripe (3) we get the following integral equation:

$$\int_{-a/2}^{a/2}dx'\,K(x,x')F(x')=0, \qquad (7)$$

with the kernel

$$K(x,x')=2\pi G(x,0|x',0). \qquad (8)$$

The nonessential factor 2π is included for the sake of convenience.

This integral equation is our main instrument. Note that taking the derivative of Eq. (5) over y and equating it to the perimeter function on the stripe, one more integral equation can be obtained. In our case it is not necessary, because our stripe antidot has no inner region, and consequently, there are no spurious eigenstates, which have to be properly eliminated in the case of other antidots.[8]

In order to fix the kernel we have to solve the Green's function equation (4). The solution of it is known[7] as

$$G(\mathbf{r}|\mathbf{r}')=-\frac{1}{2\pi}\exp\{i[\mathbf{r}\times\mathbf{r}']_z/2\}g(s), \qquad (9a)$$

$$g(s)=-\Gamma(-\varepsilon)\exp(-s/2)U(-\varepsilon|1|s), \qquad (9b)$$

$$s=|\mathbf{r}-\mathbf{r}'|^2/2, \qquad (9c)$$

$$\varepsilon=E-1/2. \qquad (9d)$$

Here the symbol $\Gamma(z)$ stands for Γ function, and $U(a|b|z)$ is the Kummer function of the second kind—the solution of the confluent hypergeometric equation.[9]

Inserting the above expression into Eq. (8), we obtain the following kernel:

$$K(x,x')=-g(s), \quad s=\frac{1}{2}(x-x')^2. \qquad (10)$$

III. SHORT STRIPE

When solving integral equation (7) numerically the main problem is the kernel singularity at $x=x'$. One can expect that it will lead to the singularity of the perimeter function at the ends of the stripe $x=\pm a/2$. In order to reveal the above singularity we considered the limit case of the ultrashort stripe ($a\to0$) when the Kummer function can be replaced by its following expansion:

$$\lim_{s\to0}U(-\varepsilon|1|s)=-\frac{1}{\Gamma(-\varepsilon)}\{\ln s+\psi(-\varepsilon)-2\psi(1)\}. \qquad (11)$$

Here the symbol $\psi(z)$ stands for the logarithmic Γ-function derivative, or the so-called ψ function. Note apart the singular logarithmic term we included terms which are large close to the first Landau level ($\varepsilon\to0$), and the constant term $\psi(1)=-\gamma$ ($\gamma\approx0.5772$), which we need to get the proper behavior of the lowest antidot energy branch.

Now inserting the above expansion into Eqs. (10), then into Eq. (7), and scaling the variables $x\to ax$, we arrive at the following approximate integral equation for the ultrashort stripe case:

$$\int_{-1/2}^{1/2}dx'\ln|x-x'|F(x')=\lambda\int_{-1/2}^{1/2}F(x')dx', \qquad (12)$$

where

$$\lambda=-\frac{1}{2}\{\ln(a^2/2)+\psi(-\varepsilon)+2\gamma\}. \qquad (13)$$

Thus, the short stripe energy spectrum problem is reduced to the calculation of the eigenvalues of integral equation (12). Then the energy can be obtained by solving algebraic equation (13). For instance, replacing the ψ function by its simplest expansion in the vicinity of the first Landau level $\psi(-\varepsilon)\approx1/\varepsilon-\gamma$, we get

$$E-1/2=\varepsilon=\frac{1}{\gamma-2\lambda-\ln(a^2/2)}. \qquad (14)$$

Due to the average of the eigenfunction over the stripe on the right-hand side of Eq. (12) it has the single not equal to zero eigenvalue λ. It can be checked by the straightforward integration that the function

$$F(x)=1/\sqrt{1/4-x^2} \qquad (15)$$

satisfies integral equation (12) with $\lambda=-2\ln2$. The corresponding energy spectrum branch is shown in Fig. 2 as a function of the stripe length a: the solid curve is obtained by the numerical solution of Eq. (13), while the dotted curve indicates the simplified version of the asymptotics according to Eq. (14). Both of them coincide in the limit case $a\to0$. We see that the antidot (short impenetrable stripe) expels a single level from the first degenerate Landau state (indicated by a thick dashed horizontal line). The longer the stripe is, the higher is the level. Note a rather fast energy grow at small a values. It is a characteristic feature of the energy
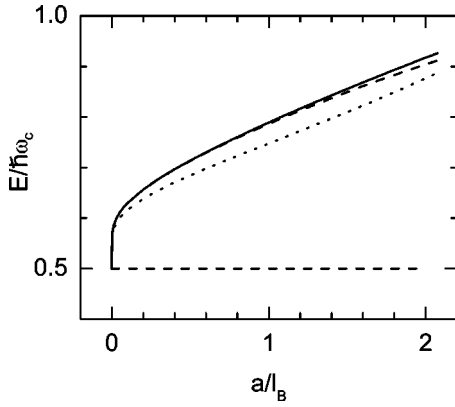
FIG. 2. Energy spectrum of ultra short stripe. Solid curve–solution of Eq. (13), dotted curve–simplified asymptotics according to Eq. (14), and dashed curve–numerical integration of integral equation (7).

level corresponding to the nonperturbed level with zero-orbital momentum, which has a nonzero electron density at the origin $\mathbf{r}=0$. All other nonperturbed levels have zero electron density there, and thus, they are weakly influenced by the stripe, and consequently, not expelled in this simplest ultrashort stripe approach.

IV. NUMERICAL RESULTS

The most important result for the ultrashort stripe case presented in the preceding section is perimeter function (15) which singularity at the stripe ends is caused by the interplay of the logarithmic singularity of the kernel and the sharp antidot edges. Thus, it is inherent to the perimeter function of general integral equation (7) as well. That is why in order to achieve the proper accuracy in numerical solution of the above equation one has to take both singularities (kernel and perimeter function) into account explicitly. For this purpose we have replaced the perimeter function as follows:

$$F(x) = \frac{f(x)}{\sqrt{a^2/4 - x^2}}, \qquad (16)$$

and discretized the obtained integral equation for the function $f(x)$ including the singular factors into the proper weights of the discretization scheme. See the details of the calculation in the Appendix. Instead of solving the obtained matrix equation

$$\mathcal{K}\mathbf{f} = 0, \qquad (17)$$

the corresponding eigenvalue problem

$$\mathcal{K}\mathbf{f}_n = \lambda_n \mathbf{f}_n \qquad (18)$$

for various electron energies ε was considered. The electron energy was defined by zeroing the obtained eigenvalues $\lambda_n = \lambda_n(\varepsilon) = 0$.

The obtained stripe energy spectrum is shown in Fig. 3 where six highest levels expelled from each Landau level (dashed horizontal lines) are indicated. On the axes the original dimensions are shown. Thus, not only the energy depen-
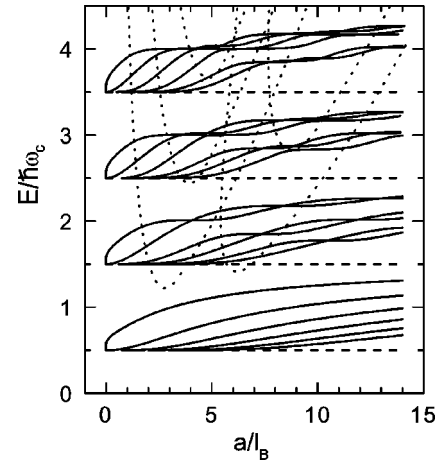

FIG. 3. Energy spectrum of the stripe. The non-perturbed Landau levels are indicated by thick dashed horizontal lines. The solutions of Eqs. (36) and (38) are indicated by dotted curves.

dence on the stripe length, but its dependence on the magnetic-field strength ($a/l_B \sim \sqrt{B}$) can also be traced.

For a comparison the spectrum of round impenetrable antidot with a diameter a is shown in Fig. 4. It was obtained by means of zeroing the radial antidot wave function [it coincides with Green's function (9) with $\mathbf{r}'=0$ assumed] at the antidot border $r=a/2$.

The characteristic feature of both spectra is the fast expelled first antidot level for each Landau state in the case of small a values. The detailed behavior of this level expelled from the first Landau level for the stripe is shown in Fig. 2 by a dashed curve. Rather good coincidence of it with the short stripe energy (solid curve) confirms a good accuracy of the developed numerical scheme.

We see that these two spectra of the antidot stripe and the round antidot differ essentially. The round antidot spectrum is a typical one for the system with separable variables. In this case the variables can be separated due to the cylindric symmetry of the problem, and actually we have independent radial problems for every angular momentum value, which energy spectrum branches freely intersect each other. The
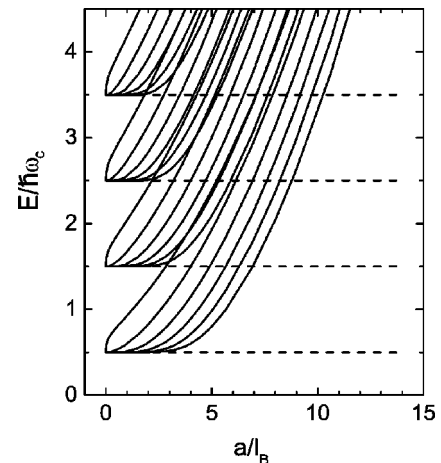

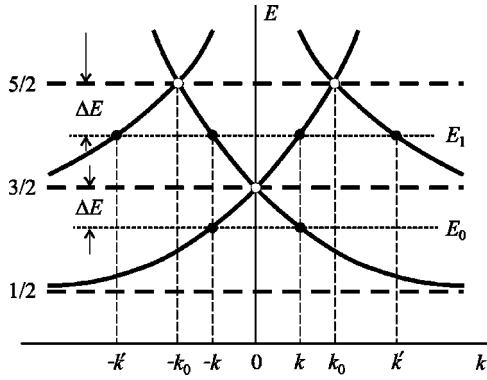FIG. 4. Energy spectrum of the round antidot.

FIG. 5. Spectrum of the magnetic edge modes.

main point is that when the antidot level with some orbital momentum l reaches the next Landau level, the antidot level with the same momentum l is already expelled from it. Consequently, any antidot level freely crosses any Landau level. And we see the energy spectrum branches going up when a increases with numerous crossings.

This is not the case for a stripe spectrum. Due to the lack of symmetry the orbital momentum is not a good quantum number any more, and instead of crossings we have anticrossings. Moreover, expelled antidot levels cannot cross the Landau levels any more. So, when the parameter a/l_B grows, the expelled antidot levels saturate bellow the next Landau level.

Nevertheless, there are still some crossings. See, for instance, the behavior of levels expelled from the second Landau level in Fig. 3. The matter is that the stripe in the perpendicular magnetic field still has the inversion symmetry ($\mathbf{r} \rightarrow -\mathbf{r}$). Due to it all the perimeter functions (and the wave functions as well) can be divided into the symmetric and the antisymmetric ones which actually satisfy the different integral equations. Thus, in the energy spectrum of the stripe crossings between the symmetric and antisymmetric spectrum branches are possible. These crossings and the occurring waviness of the spectrum branches are the most prominent feature of the considered stripe spectrum. Note that when the electron energy grows, the above waviness is transformed into numerously pronounced plateaux on the spectrum branches. Now we are going to explain the physical meaning of these plateaux and waviness considering two limit cases of the long stripe and large electron energies.

V. LONG STRIPE

Let us start with the long stripe approximation. When the stripe is infinite there are two types of magnetic edge modes propagating along the stripe on both of its sides. In this case we have the problem invariant under the translation along the stripe, and thus, the corresponding eigenvalues can be labeled by the electron momentum component k along x direction. The eigenfunctions can be expressed in terms of parabolic cylinder function as $\Psi(k|\mathbf{r}) = \exp(\pm ikx)D_\varepsilon\{\pm\sqrt{2}(y-k)\}$.[10] The spectrum is obtained by zeroing the wave function on the stripe $D_\varepsilon(\mp\sqrt{2}k) = 0$, and it is shown in Fig. 5. We see that it consists of two independent system of

branches describing the electron motion to the left above the stripe, and to the right—below it. In the asymptotic region $k \rightarrow \pm\infty$, the branches tend to the Landau levels shown by thick dashed horizontal lines. The intersection points of the above branches coincide with the Landau levels as well.

In the case of the finite stripe the electron motions above and under the stripe are no more independent, because moving above the stripe the electron reaches its end, bends around the corner, continues its motion under the stripe, and so on. Bending of the corner is a rather complicated diffraction problem, but in the asymptotic long stripe case, we can replace it by some scattering matrix acting on the longitudinal motion exponents.

The description of electron motion depends on the number of edge modes participating in it. For instance, if the electron energy is lower than the second Landau level with energy 3/2 (see, the lower thin dotted horizontal line in Fig. 5 labeled by E_0) there are only two edge modes indicated by solid circles. One of them with momentum k moves above the stripe to the left, while the other one with momentum $-k$ moves to the right under it. At the stripe ends these edge modes are scattered into one another. Since there is a single scattering channel only, the scattering probability is equal to unity. Consequently, due to the scattering event the electron wave function is multiplied by some scattering amplitude $S = \exp\{i\chi(\Delta E)\}$, while the propagation along the stripe can be taken into account by the propagator $\exp(ika)$. Thus, taking into account the periodic motion of the electron (after bending both stripe ends the exponential part of the electron wave function must coincide with itself), we can write down the following simple rule for quantization of the edge modes in the asymptotic long stripe case: $\exp\{2i(ka+\chi)\} = 1$, or

$$ka + \chi(\Delta E) = \pi n, \quad n = 1,2,\ldots. \tag{19}$$

Now using the relation $\Delta E = vk$ ($v = 5/4\sqrt{2}$) which follows from the properties of the parabolic cylinder functions close to the intersection point at $E = 3/2$, $k = 0$, and the expansion

$$\chi(\Delta E) = \chi_0 + \chi_1 \Delta E, \tag{20}$$

we solve Eq. (19) and get

$$\Delta E_n = \frac{A(n - \Delta)}{a + \delta}, \quad A = \frac{4\pi\sqrt{2}}{5} \approx 3.55. \tag{21}$$

Two other parameters: the effective elongation of the stripe $\delta = v\chi_1$ and the quantum number defect $\Delta = \chi_0/\pi$ depend on the scattering amplitude phase and unfortunately, cannot be found analytically.

Fitting the numerically obtained energy branches expelled from the first Landau level in the interval $50 < a < 100$ by $E = A_n/(a + \delta_n)$ we have obtained the following parameters:

n	1	2	3	4	5	6
δ_n	4.29	5.53	5.69	7.25	7.99	9.49
A_n	3.48	7.04	10.40	14.01	17.39	20.99
A_n/A	0.99	1.98	2.92	3.93	4.89	5.88

Note the numbers in the last row coincide rather well with the integers n what convince us that the picture of quantized edge modes is quite adequate.

To explain the behavior of energy branches expelled from the upper Landau levels is more complicated because there are more edge modes present. For instance, close to the third Landau level (see the upper thin dotted horizontal line in Fig. 5 labeled by E_1) there are four edge modes. Two of them with momenta $-k$ and k' propagate above the stripe to the left, while the other two with momenta k and $-k'$ propagate under it to the right. Consequently, in this case the propagation of electron on both sides of the stripe has to be described by the following propagator:

$$\mathcal{P}(x) = \begin{pmatrix} e^{-ikx} & 0 \\ 0 & e^{ik'x} \end{pmatrix} \qquad (22)$$

acting on the state vector

$$\Psi = \begin{pmatrix} A \\ B \end{pmatrix} \qquad (23)$$

composed of edge mode superposition coefficients. Bending of the edges is characterized by some 2×2 scattering matrix $\mathcal{S}$. Now the quantization is performed by the following self-consistency condition:

$$\mathcal{S}\mathcal{P}(a)\mathcal{S}\mathcal{P}(a)\Psi = \Psi, \qquad (24)$$

and the energy spectrum of the stripe can be defined by zeroing the determinant of the above equation,

$$\det|\mathcal{S}\mathcal{P}(a)\mathcal{S}\mathcal{P}(a) - \mathcal{I}| = 0. \qquad (25)$$

The absolute values of the scattering matrix $\mathcal{S}$ elements are given in Ref. 10. We see that close to the third Landau level the absolute value of the off-diagonal elements are nearly unity ($|S_{01}| = |S_{10}| \approx 1$), while the diagonal elements are small $|S_{00}| = |S_{11}| \approx \Delta k/2k_0$, where the symbol k_0 stands for the edge mode intersection point and $\Delta k = k' - k$ is the difference of edge mode momenta, propagating on both sides of the stripe. Thus, adding the phases, we construct the following scattering matrix:

$$\mathcal{S} = e^{i\Phi}\begin{pmatrix} e^{i\varphi}\Delta k/2k_0 & e^{i\psi} \\ e^{-i\psi} & -e^{-i\varphi}\Delta k/2k_0 e^{i\varphi} \end{pmatrix}, \qquad (26)$$

which satisfies the unitarity condition $\mathcal{S}\mathcal{S}^+ = \mathcal{I}$ with the accuracy of Δk terms.

Now expanding the momenta close to the intersection points as

$$k = k_0 - \frac{1}{v_1}\Delta E, \quad k' = k_0 + \frac{1}{v_2}\Delta E, \qquad (27a)$$

$$k' - k = \frac{2}{v'}\Delta E, \quad v' = \frac{1}{2}\left(\frac{1}{v_1} + \frac{1}{v_2}\right)^{-1}, \qquad (27b)$$

we transform Eq. (25) into the following approximate equation:

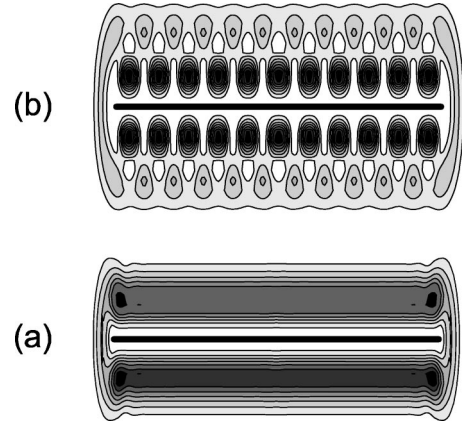

FIG. 6. Electron density for long stripe ($a/l_B = 48$): (a) – for the highest antidot level expelled from the first Landau level, and (b)— for the same level expelled from the second Landau level.

$$\exp(ia\Delta E/v') - \exp(-2i\Phi) = \pm\frac{i\Delta E}{k_0 v'}\sin(k_0 a - \varphi). \qquad (28)$$

If one neglects the small term on the right-hand side of this equation one gets the result similar to Eq. (21),

$$\Delta E_n^{(0)} = \frac{A'(n - \Delta')}{a + \delta'}, \qquad (29)$$

where $\Phi(\Delta E) = \Phi_0 + \Phi_1\Delta E$, $A' = \pi v$, $\Delta' = \Phi_0/\pi$, and $\delta' = \Phi_1 v$. The right-hand side term taken into account as a perturbation leads to the following oscillating correction:

$$\Delta E_n^{(1)} = \pm\frac{\Delta E_n^{(0)}}{k_0 a}\sin(k_0 a - \varphi). \qquad (30)$$

It is remarkable that the period of oscillations depends on $k_0 = 1/\sqrt{2}$ only. It leads to $\Delta a = 2\pi/k_0 \approx 8.89$, what coincides rather well with the period value 8.8 obtained from the numerical calculation result for the two upper levels expelled from the second Landau level.

This simple asymptotic picture of interfering magnetic edge modes is confirmed by Fig. 6 where the contour plots of the electron densities corresponding to the above considered antidot states are shown. We see that the wave function for the antidot level expelled from the first Landau level looks like a cigar (and it does not matter how long is the stripe) what indicates that it is composed of a single magnetic edge mode. In the case of the antidot level expelled from the second Landau level there are the lumps (the longer the stripe is the more lumps there are) which are caused by the interference of two pairs of edge modes propagating on both sides of the stripe.

VI. QUASICLASSICAL LIMIT

As it has already been mentioned in Sec. IV (see Fig. 3), the oscillations surveyed close to the lowest Landau levels change into well pronounced plateaux when the number of Landau level is incremented. The detailed view of the antidot
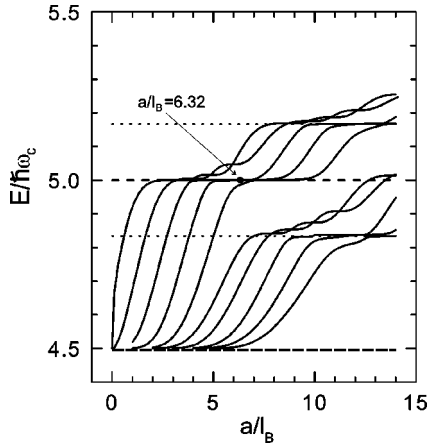
FIG. 7. The stripe energy levels expelled from the fifth Landau level.

levels expelled from the fifth Landau level is shown in Fig. 7. It is remarkable that the energy of these plateaux is very close to simple fractions of cyclotron energy. Thus, the plateau indicated by a dashed horizontal line is right in the middle between two adjacent Landau levels with energy $E = 9/2 + 1/2 = 5$, while the energy of two other plateaux indicated by dotted horizontal lines exceed the fifth Landau level energy (9/2) by one and two thirds.

Unfortunately, in the case of high Landau levels the number of the interfering edge modes is large, and this fact makes it difficult to apply the long stripe approximation considered in the preceding section. Nevertheless, the simplified description is still possible due to the large electron energy.

It is known that when the electron energy is large the quasiclassical approach based on the Bohr quantization rule can be used. In the case of free 2D electron in the homogeneous perpendicular magnetic field it reduces to the estimation of the following integral:

$$\oint \xi d\eta = 2\pi n + \pi, \quad n = 0,1,2,\ldots \quad (31)$$

composed of fast coordinates[11]

$$\xi = p_x - y/2, \quad \eta = p_y + x/2 \quad (32)$$

over the electron trajectory. Inserting the solution $\xi = \sqrt{2E}\cos t$, $\eta = \sqrt{2E}\sin t$ into Eq. (31) one immediately gets a well-known expression for Landau-level energy $E_n = n + 1/2$. Note the considered electron motion is two dimensional, and consequently, two more coordinates—the slow motion coordinates

$$X = x/2 - p_y, \quad Y = y/2 + p_x \quad (33)$$

—have to be taken into account. In free electron case it is trivial because the Hamiltonian does not depend on them. The single important thing is the commutator $[X,Y] = i$, which shows that the total slow coordinate phase volume divided by 2π gives the degeneracy of the corresponding energy level.

The influence of the stripe on the classical electron trajectory can be taken into account via scattering events. The
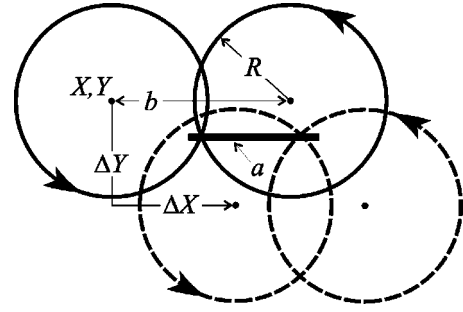

FIG. 8. Two circle trajectory.

simplest trajectory with two scattering events is shown in Fig. 8 by a solid curve. We see that in this case the trajectory is composed of two Larmor circles, and consequently, it is twice longer than the trajectory of the free electron rotating in the magnetic field. Thus, the integral on the left-hand side of Eq. (31) becomes twice larger. This fact leads to the twice smaller separation of energy levels ($\Delta E = 1/2$) as compared with the separation of Landau levels.

In order to decide whether the fractal Landau levels obtained in this quasiclassical way can take place or not, one has to inspect the slow motion coordinates. We shall take them into account in the most simple way. Note that there are more equivalent trajectories with two scattering events and the same energy (the same radius of the Larmor circle). Let us mark them by the position of the left circle center (X,Y). So, changing the center by some $(\Delta X, \Delta Y)$ we obtain another equivalent trajectory, as is shown in Fig. 8 by a dashed curve. Thus, the integral over all possible coordinates X and Y,

$$V_2(R,a) = \int\int dXdY = \int dY n_2(R, 2\sqrt{R^2 - Y^2}), \quad (34a)$$

$$n_2(R,b) = (2b - a)\Theta(2b - a)\Theta(a - b) + a\Theta(b - a) \quad (34b)$$

gives the total phase volume for the trajectories with the given radius R. Here b is the distance between the centers of both circles. We assume that the quantity $N_2(E,a) = V_2(R,a)/2\pi$ gives the degeneracy of the quasiclassical antidot level with the given energy $E = R^2/2$. The integral in Eq. (34) can be easily calculated, and it leads to the following number of degeneracy of quantum level corresponding to the classical two-circle trajectory:

$$N_2(E,a) = \frac{2E}{\pi}\rho_2(a/\sqrt{8E}), \quad (35a)$$

$$\rho_2(x) = \zeta(x)\Theta(1 - x) + \frac{\pi}{2}\Theta(x - 1) - \zeta(x/2), \quad (35b)$$

$$\zeta(x) = \arcsin x + x\sqrt{1 - x^2}. \quad (35c)$$

If the above number is less than unity, the level does not manifest itself. The energy values obtained by solving the equation
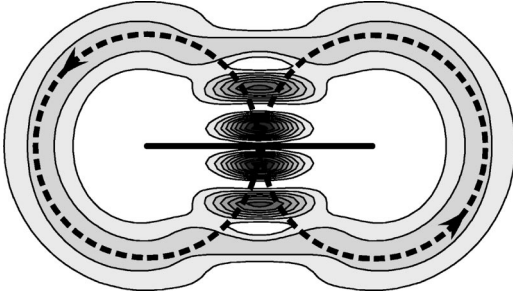
FIG. 9. Electron density for the level indicated by short dash in Fig. 7 corresponding to the classical two-circle trajectory.

$$N_2(E,a)=n, \quad n=1,2,3 \tag{36}$$

are indicated in Fig. 3 by dotted curves on its left side. We see that the larger is the energy the longer is the fractal plateau corresponding to the quasiclassical level, and the higher is its degeneracy. Moreover, there is a good coincidence of dotted curves with the plateaux ranges obtained by the numerical calculation.

In a similar way the phase volume and the degeneracy of the quasiclassical levels corresponding to three circle classical trajectories can be estimated. In this case one can obtain

$$n_3(R,b)=\Theta(2R-b)\Theta(a-b)\Theta(3b-a)$$
$$\times(a-b)\Theta(2b-a)+(3b-a)\Theta(a-2b), \tag{37a}$$

$$N_3(E,a)=\frac{E}{3\pi}\rho_3(a/\sqrt{8E}), \tag{37b}$$

$$\rho_3(x)=\begin{cases} 8\zeta(x/2)-6\zeta(x/3)-2\zeta(x) & 0<x<1 \\ 8\zeta(x/2)-6\zeta(x/3)-\pi & 1<x<2 \\ 3\pi-6\zeta(x/3) & 2<x<r. \end{cases} \tag{37c}$$

The energy values obtained by solving the equation

$$N_3(E,a)=n, \quad n=1,2 \tag{38}$$

are shown by dotted curves on the right side of Fig. 3 as well. We see that they also correlate well with the ranges of plateaux exceeded by 1/3 and 2/3 the corresponding Landau levels.

A good agreement of all dotted curves with the degeneracy of the fractional plateaus obtained in the numerical solution of the problem convinces us of the adequacy of the considered quasiclassical quantization scheme. The above picture is confirmed by the electron-density plot presented in Fig. 9. The density is calculated for the third antidot level expelled from the fifth Landau state in the case $a/l_B=6.32$ indicated by a small solid circle in Fig. 7. We see a rather good correlation of the electron density with the classical two-circle trajectory shown by a dotted curve in Fig. 9.

VII. CONCLUSIONS

The energy spectrum of the electron moving in the perpendicular magnetic field in a vicinity of an impenetrable stripe and the corresponding densities are calculated by making use of the integral equation technique for the antidot perimeter function (the perpendicular wave-function derivative at the antidot border). It is shown that the perimeter function singularities caused by sharp edges of the antidot can be overcome by proper discretization technique which takes explicitly into account the logarithmic singularity of the kernel and root-type singularities of the perimeter function.

The antidot in the magnetic field expels the antidot energy levels from every degenerated Landau state. In the case of the round antidot due to the circular symmetry expelled antidot levels go up when the radius of the antidot increases (or the magnetic field strength increases) and freely intersect each other and the Landau levels. In the case of the antidot stripe due to the lack of symmetry the variables cannot be separated, and nearly all crossings are replaced by the anticrossings. The expelled antidot levels cannot cross the Landau levels, and consequently, they saturate below the next Landau level when the stripe length increases.

As the antidot stripe still has the inversion symmetry only the pairs of symmetric and antisymmetric levels cross each other demonstrating the characteristic oscillations of the spectrum branches expelled from the excited Landau levels. These oscillations and the above-mentioned saturation can be explained in the asymptotic long stripe case by the interference of the magnetic edge modes.

When the electron energy increases (for the antidot levels expelled from the higher Landau levels) the above mentioned oscillations of the spectrum branches is transformed into plateaux at the fractal cyclotron energy values. It is shown that these fractal plateaux can be explained by using simple quasiclassical quantization rule, and they are related to the classical trajectories composed of several Larmor circles.

The above-mentioned fractal plateaux of energy branches have to be seen in magnetoresitance of arrays of stripe-type antidots, and the magnetization which is just proportional to the electron-energy derivative over the magnetic-field strength (in the considered case through the dimensionless stripe length a).

APPENDIX: DISCRETIZATION OF SINGULAR INTEGRAL EQUATION

In this section some details of the numerical solution of integral equation (7) are given. For sake of convenience we scale the variables $x \to ax$, and rewrite separately the equation for the symmetric and antisymmetric perimeter function

$$F^{\pm}(-x)=\frac{1}{2}\{F(x)\pm F(-x)\}. \tag{A1}$$

Now the equation reads

$$\int_0^{1/2} dx' K^{\pm}(x,x') F^{\pm}(x') = 0, \qquad (A2)$$

with the symmetric (or antisymmetric) kernel

$$K^{\pm}(x,x') = K(ax,ax') \pm K(ax,-ax'). \qquad (A3)$$

Next, we write down explicitly the singularity of the perimeter function

$$F^{\pm}(x) = \frac{f^{\pm}(x)}{\sqrt{1/2-x}}, \qquad (A4)$$

and the logarithmic singularity of the kernel

$$K^{\pm}(x,x') = 2 \ln|x-x'| + \widetilde{K}^{\pm}(x,x'), \qquad (A5)$$

where the second part of the kernel $\widetilde{K}^{\pm}$ is a regular function at $x=x'$. It enables us to rewrite the integral equation as follows:

$$\int_0^{1/2} \frac{dx' \, 2 \ln|x-x'| f^{\pm}(x')}{\sqrt{(1/2-x)(1/2-x')}} + \int_0^{1/2} \frac{dx' \widetilde{K}^{\pm}(x,x') f^{\pm}(x')}{\sqrt{(1/2-x)(1/2-x')}} = 0. \qquad (A6)$$

Note both terms of the equation are divided by a factor of $\sqrt{1/2-x}$ in order to have the symmetric kernel, as the numerical calculation of the corresponding symmetric matrix eigenvalues can be performed with greater accuracy than those for the nonsymmetric one.

The discretization of Eq. (A6) has been performed as follows. The perimeter function has been replaced by vector $\mathbf{f}^{\pm} = \{f_0, f_1, \dots\}$ with components $f_n = f^{\pm}(x_n)$, and $x_n = h(n+1/2)$, $h = 1/2N$. Integral equation (A6) itself has been rewritten in the form of the following matrix equation:

$$\{\mathcal{A} + \mathcal{B}^{\pm}\} \mathbf{f}^{\pm} = 0, \qquad (A7)$$

where the corresponding matrix elements of the kernel are defined as

$$A_{nm} = \int_{nh}^{(n+1)h} dx \int_{mh}^{(m+1)h} \frac{2 \ln|x-y| dy}{\sqrt{(1/2-x)(1/2-y)}}, \qquad (A8a)$$

$$B_{nm}^{\pm} = \widetilde{K}^{\pm}(x,x') B_n B_m, \qquad (A8b)$$

$$B_n = \int_{nh}^{(n+1)h} \frac{dx}{\sqrt{1/2-x}}. \qquad (A8c)$$

Both integrals can be calculated straightforwardly, and the analytical expressions for the discretization weights obtained.

Using the discretized perimeter function $\mathbf{f}^{\pm}$ the electron wave function (and the corresponding density) has been obtained via the discretized version of Eq. (5). Calculating the wave function outside the stripe (on the stripe it is equal to zero) only the perimeter function singularity has to be taken into account. Thus, Eq. (5) can be replaced by

$$\Psi^{\pm}(\mathbf{r}) = \frac{a}{2} \sum_{n=0}^{N-1} B_n \{G(a\mathbf{r}|ax',0) \pm G(a\mathbf{r}|-ax',0)\} f_n. \qquad (A9)$$

---

*Electronic address: amatulis@takas.lt

[1] L. Jacak, P. Hawrylak, and A. Wójs, *Quantum Dots* (Springer, Berlin, 1998).

[2] P.A. Maksym, H. Imamura, G.P. Mallon, and H. Aoki, J. Phys.: Condens. Matter **12**, R299 (2000).

[3] D. Weiss, M.L. Roukes, A. Menschig, P. Grambow, K. von Klitzing, and G. Weimann, Phys. Rev. Lett. **66**, 2790 (1991); A. Lorke, J.P. Kotthaus, and K. Ploog, Phys. Rev. B **44**, 3447 (1991); D. Weiss, K. Richter, A. Menschig, R. Bergmann, H. Schweizer, K. von Klitzing, and G. Weimann, Phys. Rev. Lett. **70**, 4118 (1993).

[4] X. Kleber, G.M. Gusev, U. Gennser, D.K. Maude, J.C. Portal, D.I. Lubyshev, P. Basmaji, M. de P.A. Silva, J.C. Rossi, and Yu.V. Nastaushev, Phys. Rev. B **54**, 13 859 (1996); S. Lüthi, T. Vancura, K. Ensslin, R. Schuster, G. Böhm, and W. Klein, *ibid.* **55**, 13 088 (1997); R. Schuster, K. Ensslin, J.P. Kotthaus, G. Böhm, and W. Klein, *ibid.* **55**, 2237 (1997).

[5] G. Kirczenow, B.J. Johnson, P. Kelly, C. Gould, A.S. Sachrajda, Y. Feng, and A. Delage, Phys. Rev. B **56**, 7503 (1997).

[6] G. Kirczenow, A.S. Sachrajda, Y. Feng, R.P. Taylor, L. Henning, J. Wang, P. Zawadzki, and P.T. Coleridge, Phys. Rev. Lett. **72**, 2069 (1994); G. Kirczenow, Phys. Rev. B **50**, 1649 (1994); I.J. Maasilta and V.J. Goldman, *ibid.* **57**, R4273 (1998).

[7] K. Horngerger and U. Smilansky, Phys. Rep. **367**, 249 (2002).

[8] K. Horngerger and U. Smilansky, J. Phys. A **33**, 2829 (2000).

[9] *Handbook of Mathematical Functions*, edited by M. Abramowitz and I. Stegun (Dover, New York, 1972), Chap. 13.

[10] Y.B. Levinson and E.V. Sukhorukov, J. Phys.: Condens. Matter **3**, 7291 (1991).

[11] A. Matulis, in *Nano-Physics & Bio-Electronics: A New Odyssey*, edited by T. Chakraborty, F. Peeters, and U. Sivan (Elsevier, New York, 2002), pp. 237–255.